Hindawi Publishing Corporation
International Journal of Antennas and Propagation
Volume 2012, Article ID 170420, 11 pages
doi:10.1155/2012/170420

Research Article

Cylindrical Bending of Deformable Textile Rectangular Patch Antennas

Freek Boeykens, Luigi Vallozzi, and Hendrik Rogier

Department of Information Technology, Ghent University, St. Pietersnieuwstraat 41, 9000 Ghent, Belgium

Correspondence should be addressed to Freek Boeykens, freek.boeykens@intec.ugent.be

Received 22 November 2011; Accepted 24 January 2012

Academic Editor: Ana Collado

Textile patch antennas are well known as basic components for wearable systems that allow communication between a human body and the external world. Due to their flexibility, textile antennas are subjected to bending when worn, causing a variation in resonance frequency and radiation pattern with respect to the flat state in which their nominal design is performed. Hence, it is important for textile antenna engineers to be able to predict these performance parameters as a function of the bending radius. Therefore, we propose a comprehensive analytical model that extends the cylindrical cavity model for conformal rigid patch antennas by incorporating the effects of patch stretching and substrate compression. It allows to predict the resonance frequency and the radiation pattern as a function of the bending radius. Its validity has been verified experimentally. Unlike previous contributions, which concerned only qualitative studies by means of measurements and numerical full-wave simulations, the proposed model offers advantages in terms of physical insight, accuracy, speed, and cost.

1. Introduction

Textile antennas emerged during the last decade as a new promising class of antennas that are particularly suitable for use in wearable applications [1–5]. These antennas can be fully integrated into intelligent garments, known as *wearable electronic systems* [6], enabling the transmission of data collected by wearable sensors or the reception of signals sent to wearable actuators integrated into clothing. The applications of wearable systems and textile antennas are numerous, ranging from rescue workers interventions' coordination to monitoring of dependent patients in hospital and sports applications.

In order to allow an optimal integration into garments without hindering the wearer's movements and comfort, the most suitable topology for a textile antenna is the planar patch. This flexible patch may be subjected to bending when the garment is worn, conforming its shape to the surface on which it is placed. As a result, stretching of the patch (resulting in an elongation of the resonant length) and substrate compression (leading to a variation of the dielectric permittivity as a function of the bending radius) can occur.

Since the beginning of textile antenna design, these effects have been taken into account, however, they were not well known and were compensated for by increasing the antenna bandwidth and validating the design afterwards by experiments [4]. Hence, it is essential to model the behaviour of the antenna under bent conditions and to predict the influence of bending on the resonance frequency and the radiation pattern. Full-wave simulation approaches are a potential solution, but most available commercial software tools do not offer the possibility of building a conformal mesh for bent structures, which results in inaccuracies in the obtained results. Moreover, these simulations do not offer physical insight into the bending mechanisms and may require high computational effort and time. Therefore, we propose analytical formulas that help the designer to assess a priori the effects of bending, stretching, and compression. The work described in this paper focuses on cylindrical bending in particular, since, for wearable applications, textile antennas are usually deployed on cylindrical surfaces such as a human arm, a leg, or a torso.

This study starts from past research efforts on rigid *conformal* antennas attached to cylindrical surfaces, of which

several contributions can be found in literature. Krowne started by extending the popular cavity model for the rectangular patch antenna (introduced by Lo et al. in 1979 [7]) to the cylindrical case [8]. Resonance frequencies for the TE_z and TM_z modes were theoretically derived, though radiation patterns were not calculated in this model. A more comprehensive study was performed by Dahele et al. [9] and Luk et al. [10]. Their cavity model is only valid for patch antennas with a very thin substrate, but resonance frequencies, far fields, input impedances, and Q-factors were derived analytically. Other analytical approaches were also introduced, which allow to calculate radiation patterns of antennas with patches of arbitrary shape [11–13]. However, they are based on an electric surface current model and assume the surface current distribution to be known on the patch.

Cylindrical bending of *deformable* textile antennas has been an important subject in recent papers, but exclusively from an experimental point of view [4, 5, 14–16]. The general conclusions drawn from these contributions are that bending causes an upward shift of the resonance frequency, a broadening of the radiation pattern, a decrease in gain along broadside, and an alteration of the polarisation (in case of a circularly polarised antenna). Yet, these studies are rather qualitative and do not provide physical insight into the complex mechanisms occurring due to antenna bending.

The present work tries to overcome all drawbacks of the previous analysis methods by proposing a comprehensive study on cylindrical bending of rectangular textile patch antennas. An analytical model based on the cylindrical cavity model for conformal antennas, which allows to calculate both the resonance frequency and the radiation pattern, is constructed. This offers the advantage of requiring only small computational effort for calculating the main antenna performance parameters.

In order to model deformable textile patch antennas, some novel extensions to rigid conformal antenna models are proposed:

(1) Wearable textile antennas are usually realised with electrotextiles as conductive patch materials, which are subjected to stretching when the antenna is bent. This causes an elongation of the patch along one direction and shifts the resonance frequency [17]. This behaviour is integrated into the model by introducing a factor that determines the location of the original patch width.

(2) Textile antennas are subjected to compression when bent, which causes a variation of its dielectric permittivity. This can be tackled by proposing an expression for the compressed permittivity $\epsilon_{r,\text{comp}}$ as a function of the bending radius.

The model is validated by means of

(1) theoretical validation for large curvature radii using Debye's expansion for large-order Bessel functions;

(2) experimental validation by measuring five prototypes based on different substrates with different thicknesses, patch materials, and operation frequencies.

The organisation of the paper is as follows. First, the cavity model for cylindrical-rectangular antennas is described in Section 2. The expressions for the resonant fields inside the cavity are calculated, from which the resonance frequencies and radiation patterns are derived. In Section 3, the cavity model is verified for large curvature radii by comparing the obtained dispersion relations with the expression for resonance frequencies in rectangular cavities. Section 4 presents the experimental results. The proposed model is verified by means of five textile antenna prototypes with different geometries and material characteristics. Both resonance frequencies and radiation patterns are compared. Finally, the general conclusions are summarised in Section 5.

2. Theory

The geometry of the cylindrical cavity representing the textile antenna is shown in Figure 1. The length and width of the wearable antenna are denoted by L and W, and the flexible dielectric substrate has a height h and relative permittivity ϵ_r. The curvature radius is a, and the angle formed by the edges of the patch is β.

In order to obtain a relationship between W, a, and β, one has to take into account whether the antenna patch is stretchable or not. According to [17], the following relations exist for stretchable patches:

$$\frac{\Delta W}{W} = \frac{h}{2a+h}, \tag{1a}$$

$$\beta(a+h) = W + \Delta W, \tag{1b}$$

with $W + \Delta W$ the width of the bent patch. This is shown in Figure 2. Combining (1a) and (1b) leads to

$$\beta\left(a + \frac{h}{2}\right) = W. \tag{2}$$

This means that the original patch width is located at $\rho = a+h/2$ due to patch elongation. If the patch is nonstretchable, the patch length does not vary when bending the antenna and groundplane crumpling occurs. The original width W is then still located at $\rho = a + h$.

Because textile antennas can be constructed using both stretchable and nonstretchable patches, we introduce a factor d (Figure 2) that determines the location of the original width:

$$W = \beta(a + hd). \tag{3}$$

This factor d can take values between 0.5 and 1. For perfectly stretchable patches we find that $d = 0.5$ and for perfectly nonstretchable patches $d = 1$.

2.1. The Cavity Model. We now proceed with the derivation of the cylindrical cavity model [8]. The cavity is bounded by electric walls at $\rho = a$ and $\rho = a + h$ and magnetic walls at $\phi = \pm\beta/2$ and $z = \pm L/2$.

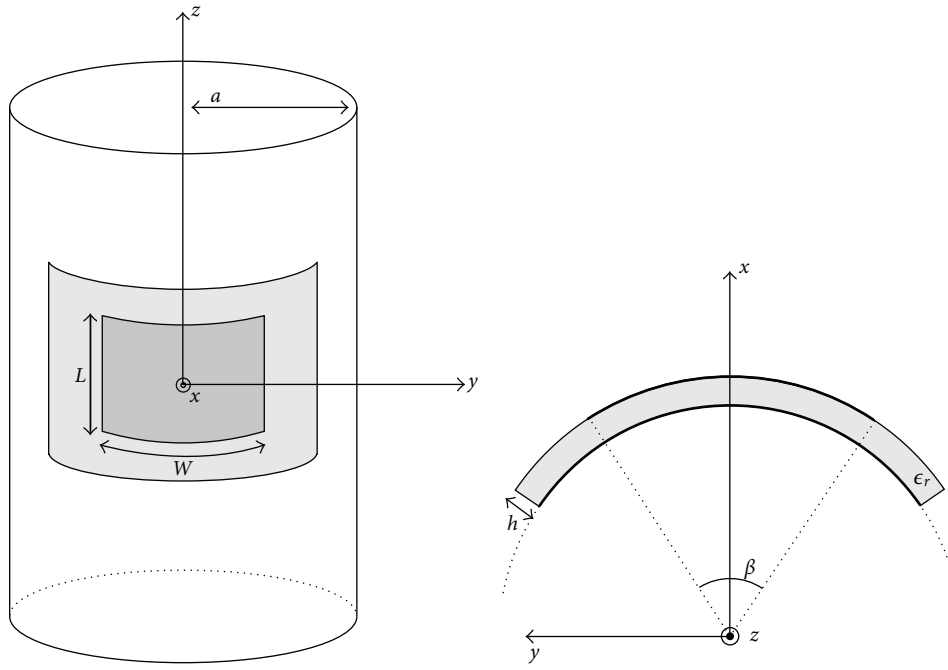

Figure 1: Geometry of the cavity: top view (a) and side view (b).

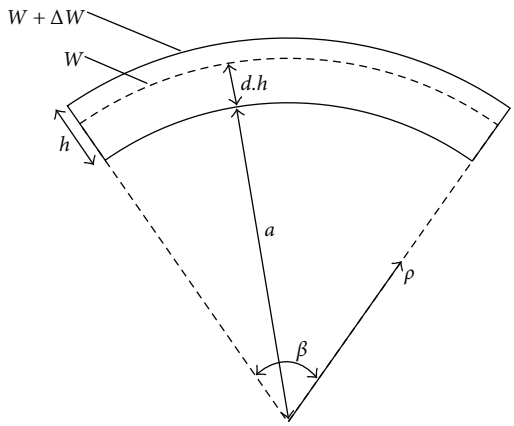

Figure 2: Patch elongation.

The electric and magnetic fields inside the cavity are given by

$$\mathbf{E} = -\nabla \times \mathbf{F} - j\omega\mu\mathbf{A} + \frac{1}{j\omega\epsilon}\nabla(\nabla \cdot \mathbf{A}), \tag{4a}$$

$$\mathbf{H} = \nabla \times \mathbf{A} - j\omega\epsilon\mathbf{F} + \frac{1}{j\omega\mu}\nabla(\nabla \cdot \mathbf{F}), \tag{4b}$$

where, given the translation invariance of the structure, the vector potentials are defined by

$$\begin{aligned} \mathbf{A} &= A_z\mathbf{u}_z, \\ \mathbf{F} &= F_z\mathbf{u}_z. \end{aligned} \tag{5}$$

The scalar wave functions A_z and F_z obey the scalar Helmholtz equation

$$\nabla^2\psi + k^2\psi = 0, \tag{6}$$

with $k^2 = \epsilon_r k_0^2$.

After separation of variables in cylindrical coordinates, the TE_z solution is found by choosing $\mathbf{A} = 0$. Applying the boundary conditions leads to

$$\psi = R_{k_\phi}\left(k_\rho\rho\right)\sin\left(\frac{m\pi}{\beta}\phi + \frac{m\pi}{2}\right)\cos\left(\frac{n\pi}{z}z + \frac{n\pi}{2}\right), \tag{7}$$

where

$$\begin{aligned} R_{k_\phi}\left(k_\rho\rho\right) &= c_{\mathrm{TE}}\left(Y'_{k_\phi}\left(k_\rho a\right)J_{k_\phi}\left(k_\rho\rho\right) - J'_{k_\phi}\left(k_\rho a\right)Y_{k_\phi}\left(k_\rho\rho\right)\right), \\ k_\phi &= \frac{m\pi}{\beta}, \\ k_z &= \frac{n\pi}{L}, \\ k_\rho &= \sqrt{k^2 - k_z^2}. \end{aligned} \tag{8}$$

The TM_z solution can be found by choosing $\mathbf{F} = 0$. Applying the boundary conditions leads to

$$\psi = R_{k_\phi}\left(k_\rho\rho\right)\cos\left(\frac{m\pi}{\beta}\phi + \frac{m\pi}{2}\right)\sin\left(\frac{n\pi}{z}z + \frac{n\pi}{2}\right), \tag{9}$$

where

$$R_{k_\phi}\left(k_\rho\rho\right) = c_{\mathrm{TM}}\left(Y_{k_\phi}\left(k_\rho a\right)J_{k_\phi}\left(k_\rho\rho\right) - J_{k_\phi}\left(k_\rho a\right)Y_{k_\phi}\left(k_\rho\rho\right)\right). \tag{10}$$

The constants c_{TE} and c_{TM} are proportionality coefficients for the TE_z and the TM_z modes, respectively. Further in this paper, the TE_z and TM_z modes will also be referred to as the TE_{mn} and the TM_{mn} modes.

2.2. Resonance Frequency. The dispersion relations are found by imposing all boundary conditions. For the TE_z modes, the dispersion relation becomes

$$J'_{k_\phi}\left(k_\rho a\right)Y'_{k_\phi}\left(k_\rho(a+h)\right) = J'_{k_\phi}\left(k_\rho(a+h)\right)Y'_{k_\phi}\left(k_\rho a\right). \tag{11}$$

For the TM_z modes, one finds

$$J_{k_\phi}\left(k_\rho a\right)Y_{k_\phi}\left(k_\rho(a+h)\right) = J_{k_\phi}\left(k_\rho(a+h)\right)Y_{k_\phi}\left(k_\rho a\right). \tag{12}$$

The resonance frequencies are found as zeros of these equations.

2.3. Radiation Pattern. The radiation pattern can be calculated from the equivalent magnetic currents $\mathbf{M} = E_\rho \mathbf{u}_\rho \times \mathbf{u}_n$ along the edges of the curved patch [10, 18].

In general, E_ρ can be written as

$$E_\rho = \lambda(\rho)\cos\left(\frac{m\pi}{\beta}\phi + \frac{m\pi}{2}\right)\cos\left(\frac{n\pi}{L}z + \frac{n\pi}{2}\right), \tag{13}$$

where $\lambda(\rho)$ is a mode-dependent factor. For the TE_z modes, $\lambda(\rho)$ is defined as

$$\lambda_{\mathrm{TE}}(\rho) = -\frac{1}{\rho}\frac{m\pi}{\beta}R_{m\pi/\beta}\left(\sqrt{k^2 - \left(\frac{n\pi}{L}\right)^2}\,\rho\right). \tag{14}$$

For the TM_z modes, $\lambda(\rho)$ becomes

$$\lambda_{\mathrm{TM}}(\rho) = -\frac{j\omega}{\epsilon}\frac{n\pi}{L}\sqrt{k^2 - \left(\frac{n\pi}{L}\right)^2}\,R'_{m\pi/\beta}\left(\sqrt{k^2 - \left(\frac{n\pi}{L}\right)^2}\,\rho\right). \tag{15}$$

After some calculations, the following far-field components are found:

$$E_\theta = \frac{\lambda(a+h)}{2\pi^2\sin\theta}\frac{e^{-jk_0 r}}{r}\sigma(n, -Lk_0\cos\theta) \cdot \sum_{p=-\infty}^{+\infty}\frac{e^{jp\phi}j^{p+1}I(m,p,\beta)}{H_p^{(2)}((a+h)k_0\sin\theta)}, \tag{16a}$$

$$E_\phi = j\frac{\lambda(a+h)}{2\pi^2}\frac{e^{-jk_0 r}}{r} \cdot \sum_{p=-\infty}^{+\infty}\frac{e^{jp\phi}j^{p+1}}{H_p^{(2)\prime}((a+h)k_0\sin\theta)} \times \left(\sigma(m,p\beta)I(n,-k_0\cos\theta,L) - \frac{p\cos\theta\;\sigma(n,-Lk_0\cos\theta)I(m,p,\beta)}{(a+h)k_0\sin^2\theta}\right) \tag{16b}$$

with

$$\begin{aligned}\sigma(q,a) &= (-1)^q e^{-ja/2} - e^{ja/2},\\ I(q,a,b) &= \int_{-b/2}^{b/2}\cos\left(\frac{q\pi}{b}x + \frac{q\pi}{2}\right)e^{-jax}\mathrm{d}x,\\ &= j\frac{ab^2\;\sigma(q,ab)}{a^2b^2 - q^2\pi^2}.\end{aligned} \tag{17}$$

3. Validation of the Model for Large Curvature Radii

Now, the analytical model will be verified for the limit case where the curvature radius a tends to ∞. A rectangular cavity is then obtained, and the following relation should be found:

$$k^2 = \left(\frac{m\pi}{W}\right)^2 + \left(\frac{n\pi}{L}\right)^2 + \left(\frac{l\pi}{h}\right)^2. \tag{18}$$

By rewriting (11) and (12) using the substitutions

$$\nu = \frac{m\pi}{\beta}, \tag{19a}$$

$$\sec\alpha = \sqrt{k^2 - \left(\frac{n\pi}{L}\right)^2}\,\frac{W - \beta hd}{m\pi}, \tag{19b}$$

$$\sec\gamma = \sqrt{k^2 - \left(\frac{n\pi}{L}\right)^2}\,\frac{W - \beta h(d-1)}{m\pi}, \tag{19c}$$

we obtain

$$J_\nu(\nu\sec\alpha)Y_\nu(\nu\sec\gamma) = J_\nu(\nu\sec\gamma)Y_\nu(\nu\sec\alpha), \tag{20a}$$

$$J'_\nu(\nu\sec\alpha)Y'_\nu(\nu\sec\gamma) = J'_\nu(\nu\sec\gamma)Y'_\nu(\nu\sec\alpha). \tag{20b}$$

When taking the limit for a to ∞, ν also goes to ∞, while α and γ remain constant. Debye's asymptotic expansion for large-order Bessel functions can then be utilised for $\nu \to \infty$ [19]:

$$J_\nu\left(\nu\sec\chi\right) \sim \sqrt{\frac{2}{\pi\nu\tan\chi}}\left(\cos\xi\sum_{k=0}^{\infty}\frac{U_{2k}\left(j\cot\chi\right)}{\nu^{2k}} - j\sin\xi\sum_{k=0}^{\infty}\frac{U_{2k+1}\left(j\cot\chi\right)}{\nu^{2k+1}}\right), \tag{21a}$$

$$Y_\nu\left(\nu\sec\chi\right) \sim \sqrt{\frac{2}{\pi\nu\tan\chi}}\left(\sin\xi\sum_{k=0}^{\infty}\frac{U_{2k}\left(j\cot\chi\right)}{\nu^{2k}} + j\cos\xi\sum_{k=0}^{\infty}\frac{U_{2k+1}\left(j\cot\chi\right)}{\nu^{2k+1}}\right), \tag{21b}$$

$$J'_\nu\left(\nu\sec\chi\right) \sim \sqrt{\frac{\sin 2\chi}{\pi\nu}}\left(-\sin\xi\sum_{k=0}^{\infty}\frac{V_{2k}\left(j\cot\chi\right)}{\nu^{2k}} - j\cos\xi\sum_{k=0}^{\infty}\frac{V_{2k+1}\left(j\cot\chi\right)}{\nu^{2k+1}}\right), \tag{21c}$$

$$Y'_\nu\left(\nu\sec\chi\right) \sim \sqrt{\frac{\sin 2\chi}{\pi\nu}}\left(\cos\xi\sum_{k=0}^{\infty}\frac{V_{2k}\left(j\cot\chi\right)}{\nu^{2k}} - j\sin\xi\sum_{k=0}^{\infty}\frac{V_{2k+1}\left(j\cot\chi\right)}{\nu^{2k+1}}\right), \tag{21d}$$

with

$$\xi = \nu\left(\tan\chi - \chi\right) - \frac{\pi}{4}, \tag{22}$$

and $U_k(p)$ and $V_k(p)$ polynomials in p of degree $3k$, given by $U_0(p) = V_0(p) = 1$, and

$$\begin{aligned} U_{k+1}(p) &= \frac{1}{2}p^2(1-p^2)U'_k(p) + \frac{1}{8}\int_0^p (1-5t^2)U_k(t)\,\mathrm{d}t, \\ V_{k+1}(p) &= U_{k+1}(p) - \frac{1}{2}p(1-p^2)U_k(p) \\ &\quad - p^2(1-p^2)U'_k(p). \end{aligned} \tag{23}$$

Using the lowest-order Debye's expression, one finds for both the dispersion relations:

$$\sin\xi\cos\xi' = \sin\xi'\cos\xi \tag{24}$$

with

$$\begin{aligned} \xi &= \nu(\tan\alpha - \alpha) - \frac{\pi}{4}, \\ \xi' &= \nu(\tan\gamma - \gamma) - \frac{\pi}{4}. \end{aligned} \tag{25}$$

This leads to

$$\tan\gamma - \gamma = \tan\alpha - \alpha + \frac{l}{n}\beta. \tag{26}$$

Assuming that $h \ll \lambda$, a first-order Taylor expansion can be performed on $\tan\gamma(h) - \gamma(h)$ and $\tan\alpha(h) - \alpha(h)$ for $h \to 0$. Expression (26) then becomes

$$\sin\alpha(0) = \frac{l\pi}{h}\frac{1}{\sqrt{k^2 - (n\pi/L)^2}}. \tag{27}$$

Combining (19b) and (27) results in

$$\sqrt{1 - \frac{1}{\left(k^2 - (n\pi/L)^2\right)(W/(m\pi))^2}} = \frac{l\pi}{h}\frac{1}{\sqrt{k^2 - (n\pi/L)^2}}, \tag{28}$$

which finally leads to (18) and verifies the transition to a rectangular cavity.

4. Comparison of Experimental and Theoretical Results

Using this model, the resonance frequencies and radiation patterns of flexible textile antennas can be calculated analytically. However, when comparing the measured resonance frequencies of a fabricated textile antenna with the frequencies obtained from our model for different bending radii, a discrepancy is noticed. This is due to the fact that textile antennas are subjected to compression when bent. Consequently, the substrate permittivity will change as a function of the bending radius. This effect needs to be incorporated in our model in order to provide a good prediction of the resonance frequency. In other words, an expression for the permittivity $\epsilon_{r,\mathrm{comp}}$ of a substrate subjected to compression needs to be found.

4.1. Experimental Setup. By measuring five prototypes with different specifications and constructed on different flexible materials, the effect of several parameters on $\epsilon_{r,\mathrm{comp}}$ is investigated. Their geometry is displayed in Figure 3. All prototypes are fed by a probe feed structure, with the probe located on the perpendicular bisector of the L_p edge.

Prototypes 1 and 2 are both fabricated on aramid substrates and are designed for the 1.57 GHz GPS band. The patch material of prototype 1 is the stretchable electro-textile Flectron, whereas nonstretchable copper foil is used for prototype 2. Prototypes 3, 4, and 5 are fabricated on cotton substrates and have copper foil as patch material. Prototypes 3 and 5 are designed for the 1.57 GHz GPS band, whereas prototype 4 operates in the 2.45 GHz ISM band. The difference between prototype 3 and 5 is the thickness of the substrate. The parameters of the prototypes are shown in Table 1, where the substrate height h is determined based on the ISO 5084 standard [20].

For these prototypes, the resonance frequencies in flat and bent state are measured by means of a PNA-X vector network analyser. The bent states are realised by attaching the antennas to plastic cylinders with different radii ranging from 31.5 mm to 90 mm. These radii resemble typical curvatures of human body parts.

When the antennas are bent in the W_p direction, the model is used by setting $L = L_p$ and $W = W_p$. According to the model, the TE_{10} mode is then excited and (11) needs to be solved in order to determine the resonance frequency. Similarly, when bending the antennas in the L_p direction, one has to set $L = W_p$ and $W = L_p$. According to the model, the TM_{01} mode is then excited, and the resonance frequency follows from (12).

Table 1: Parameters of the prototypes.

Prototype	1	2	3	4	5
L_p [mm]	81.2	81.2	78.5	52.5	78.5
W_p [mm]	69.25	69.25	69.3	43.7	68.3
h [mm]	2	2	2.7	2.7	4.05
y_f [mm]	16	16	17	11	16.8
ϵ_r	1.75	1.75	1.715	1.715	1.715
d	0.5	1	1	1	1

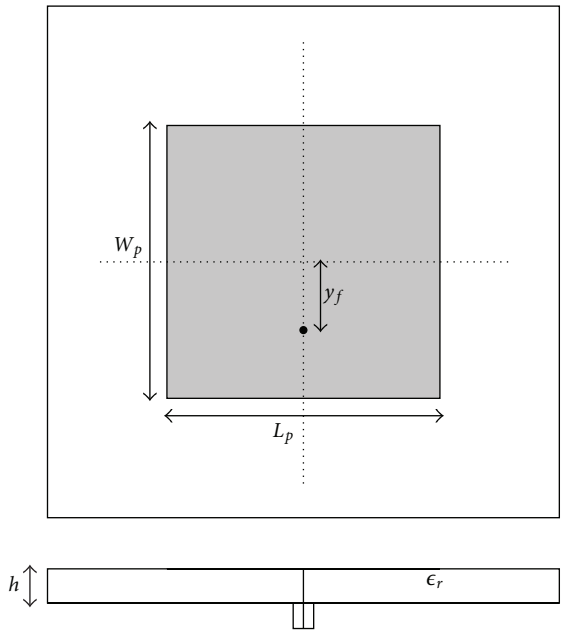

Figure 3: Geometry of a prototype.

4.2. Compression Effects on the Permittivity. After comparing the measured resonance frequencies of the prototypes for the different bending radii, the following observations are made:

(1) The $\epsilon_{r,\text{comp}}$ is inversely proportional to the bending radius a, since compression becomes stronger as the curvature radius decreases.

(2) The part of the substrate that undergoes the largest compression has a height $h(d - 0.5)$, and $\epsilon_{r,\text{comp}}$ is directly proportional to this.

(3) The compression is not frequency dependent.

Based on these observations, an empirical formula for $\epsilon_{r,\text{comp}}$ can be found:

$$\epsilon_{r,\text{comp}} = \epsilon_{r,\text{flat}}\left(1 + \eta\frac{h(d-0.5)}{a}\right). \tag{29}$$

The permittivity $\epsilon_{r,\text{flat}}$ is obtained by evaluating (18) after measuring the antenna in flat state under well-defined environmental conditions. It therefore captures effects such as humidity, temperature, and fringing effects, while the second term in (29) isolates the effect of bending. The parameter h is the height of the flexible substrate in flat state, measured according to the ISO 5084 standard. This simplifies the work of the designer, since he does not need to measure the height of the substrates for each bending radius.

Table 2: Proportionality factors η for the compression correction term.

Prototype	2	3	4	5
TE_{10} mode	1 589	1 497	1 472	1 485
TM_{01} mode	380	214	592	654

Table 3: Relative mean error between the modeled and measured resonance frequencies of the bent prototypes for the TE_{10} mode.

Prototype	1	2	3	4	5
$\tau(0)$ [%]	0.09	1.56	1.97	1.94	2.91
$\tau(\eta)$ [%]	0.09	0.03	0.09	0.07	0.12

Table 4: Relative mean error between the modeled and measured resonance frequencies of the bent prototypes for the TM_{01} mode.

Prototype	1	2	3	4	5
$\tau(0)$ [%]	0.04	0.37	0.23	0.76	1.28
$\tau(\eta)$ [%]	0.04	0.03	0.07	0.10	0.07

Expression (29) also takes into account the following remarks:

(1) When a tends to ∞, the antenna becomes planar and $\epsilon_{r,\text{flat}}$ is found.

(2) For perfectly stretchable antennas, $\epsilon_{r,\text{comp}} = \epsilon_{r,\text{flat}}$. Hence, the resonance frequency will not change when the antenna is bent.

The proportionality factor η can be found for each prototype with a nonstretchable patch by minimising an error function $\tau(\eta)$, defined by

$$\tau(\eta) = \frac{1}{N}\sum_{i=1}^{N}\frac{|f_{\text{mod},i}(\eta) - f_{\text{meas},i}|}{f_{\text{meas},i}}. \tag{30}$$

This function represents the relative mean error between the modeled and measured resonance frequencies of a bent prototype, with N being the number of cylinders.

The calculation of η is carried out iteratively by combining MATLAB's minimisation function *fminsearch* with our analytical model in Maple. The obtained values for both the TE_{10} and the TM_{01} modes are shown in Table 2. The η-values for the TE_{10} modes are quite similar, whereas the values for the TM_{01} mode exhibit larger differences. Also, there is a significant difference between the values for the TE_{10} mode and the TM_{01} mode. This is due to the geometry and feeding structure of the prototypes. The solid feed points are not located in the center of the patches and thus produce different compression effects, depending on whether the prototypes are bent in the W_p direction or the L_p direction.

Tables 3 and 4 display the error values when using $\epsilon_r = \epsilon_{r,\text{flat}}$ (shown as $\tau(0)$) and $\epsilon_r = \epsilon_{r,\text{comp}}$ (shown as $\tau(\eta)$) for the TE_{10} mode and the TM_{01} mode, respectively. A constant

small error of ca. 0.1% can be found for all prototypes when using the ideal proportionality factor η, validating the use of (29).

4.3. Resonance Frequency. Figure 4 shows the modeled and measured resonance frequencies of prototypes 1 and 3 as a function of the bending radius when the antennas are bent in the W_p direction. Prototype 1 has a stretchable patch, so patch elongation occurs and the substrate will not be compressed ($\epsilon_{r,\text{comp}} = \epsilon_{r,\text{flat}}$). Consequently, the resonance frequency almost does not change when the antenna is bent. Prototype 3 has a nonstretchable patch, therefore the resonance frequency will change with varying curvature radii. The resonance frequencies obtained from the model with and without compression correction are displayed, where the model without compression correction can be seen as if the antenna would be conformally attached to the cylinders. Since the prototypes are flexible deformable antennas, the measured curve follows the curve obtained from the model with compression correction. One also notices that the increase in resonance frequency for smaller bending radii is not as distinct as compared to the conformal case. This behaviour is also observed for the other prototypes.

In Figure 5, the modeled and measured resonance frequencies of prototypes 1 and 3 are displayed as a function of the bending radius when the antennas are bent in the L_p direction. According to the model, the resonance frequency of prototype 1 does not vary since no compression occurs and the resonant length is not bent in TM_z mode. For prototype 3, a decrease in resonance frequency now occurs for smaller bending radii. This effect is purely due to compression of the substrate, which can also be noticed by comparison with the curve obtained from the model without compression correction, where the resonance frequency does not change. Again, this result is also observed for the other prototypes.

As a footnote, we like to point out the difference in resonance frequency for the flat state between Figures 4 and 5. The measurements for the TM_z case were performed later in time than those for the TE_z case. As a result, the resonance frequencies of the prototypes have changed due to humidity effects. This effect is larger for prototype 3 than for prototype 1, since the cotton substrate suffers more from this effect than the aramid substrate [21]. However, the model still remains accurate, since it only takes into account bending effects. In other words, using this formulation, the effect of bending on the behaviour of deformable antennas can be isolated.

4.4. Radiation Pattern. Figure 6 shows the modeled and measured radiation patterns in the XY plane (as defined in Figure 1) of the stretchable prototype 1 for curvature radii of 90 mm and 31.5 mm at a frequency of 1.567 GHz (the resonance frequency of the planar antenna) when the antenna is bent in the W_p direction. The radiation pattern calculated by the model is normalised with respect to the measured gain in broadside direction, since only its shape can be predicted. For a curvature radius of 90 mm, the measured 3 dB beamwidth is 75°, and the modeled 3 dB beamwidth is 80°. For a bending

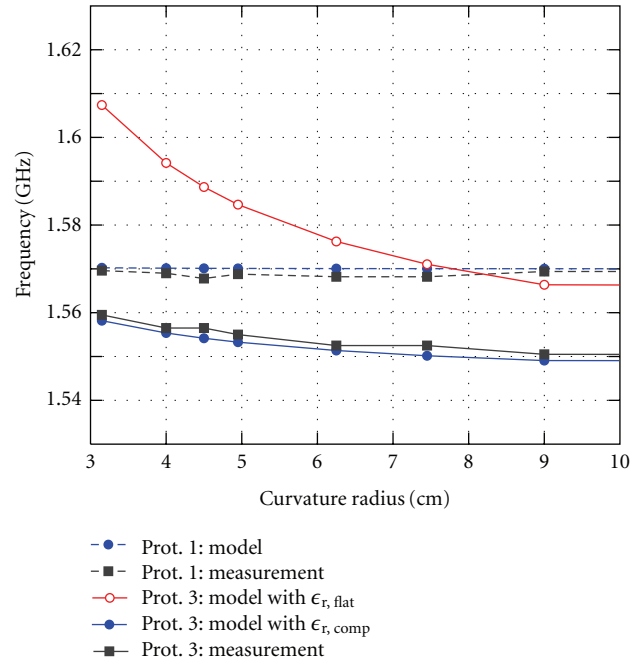

FIGURE 4: Resonance frequencies of prototypes 1 and 3 as a function of the bending radius when the antennas are bent along the W_p direction.

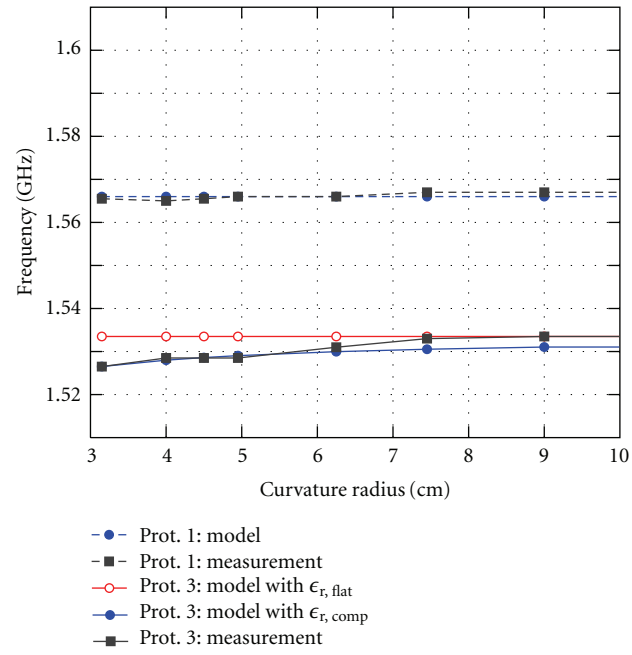

FIGURE 5: Resonance frequencies of prototypes 1 and 3 as a function of the bending radius when the antennas are bent along the L_p direction.

radius of 31.5 mm, the measured 3 dB beamwidth is 86°, and the modeled 3 dB beamwidth is 84°.

On Figure 7, the modeled and measured radiation patterns in the XY plane of the nonstretchable prototype 2 are displayed for curvature radii of 90 mm and 31.5 mm at a frequency of 1.573 GHz (the resonance frequency of

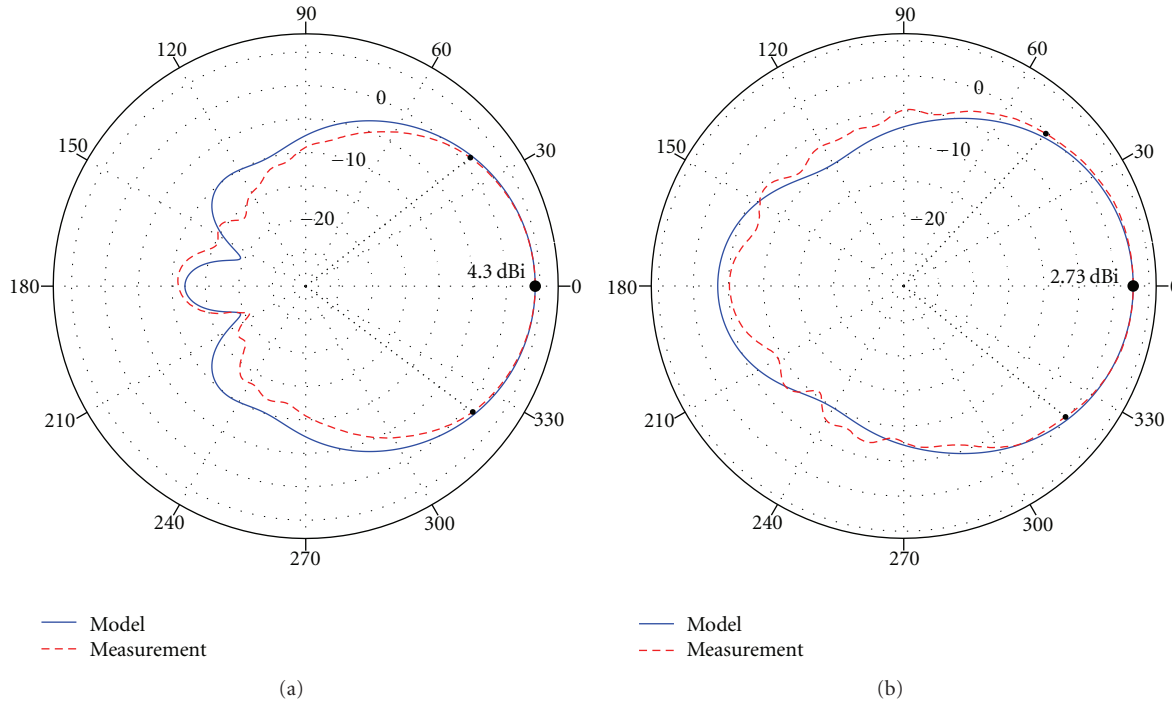

Figure 6: Radiation pattern in XY plane of prototype 1 for 1.567 GHz when bent in the W_p direction. The bending radii are 90 mm (a) and 31.5 mm (b).

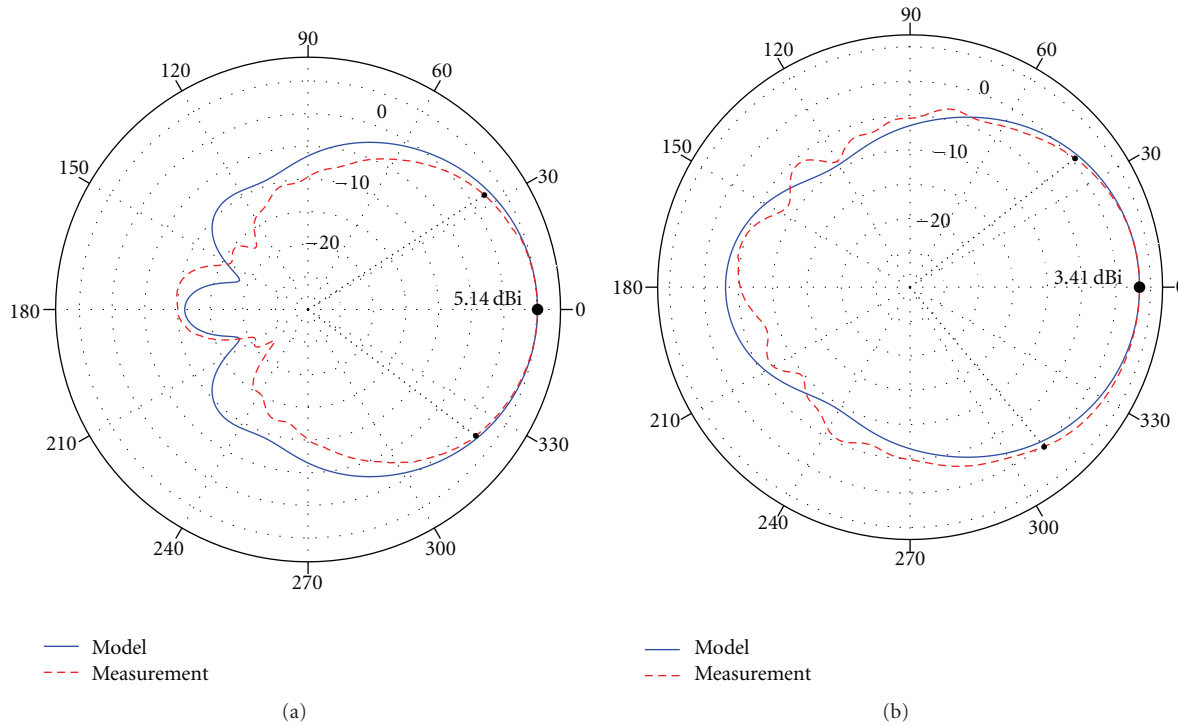

Figure 7: Radiation pattern in XY plane of prototype 2 for 1.573 GHz when bent in the W_p direction. The bending radii are 90 mm (a) and 31.5 mm (b).

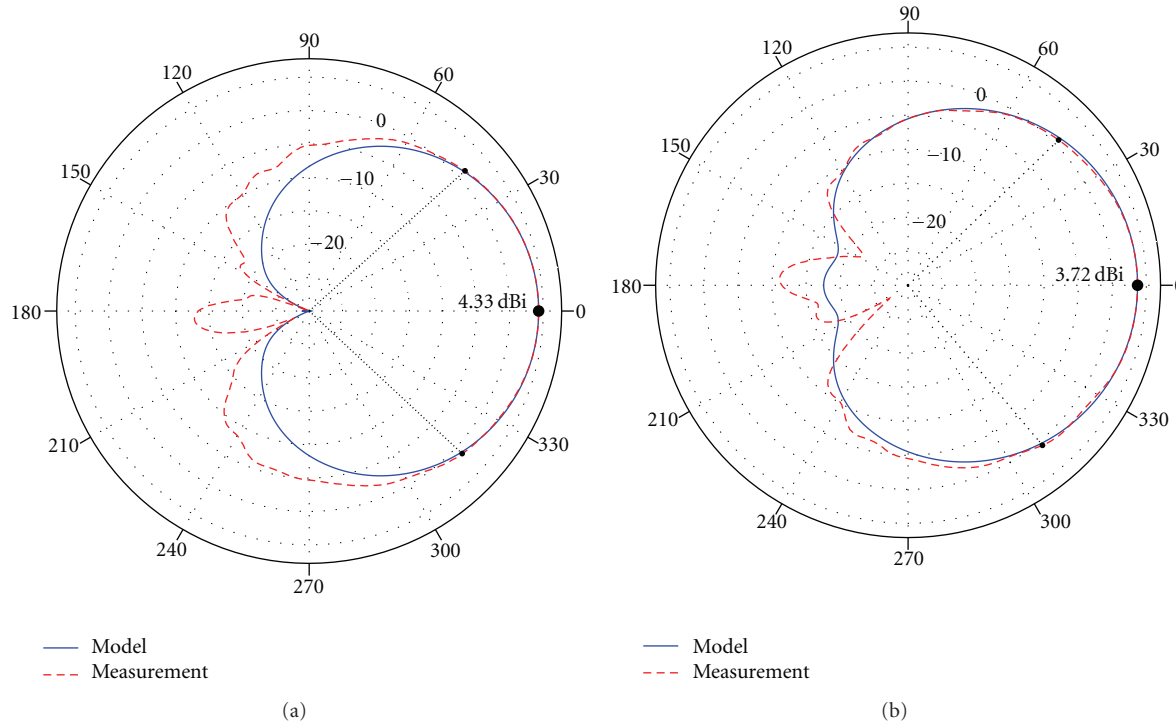

FIGURE 8: Radiation pattern in XY plane of prototype 2 for 1.573 GHz when bent in the L_p direction. The bending radii are 90 mm (a) and 40 mm (b).

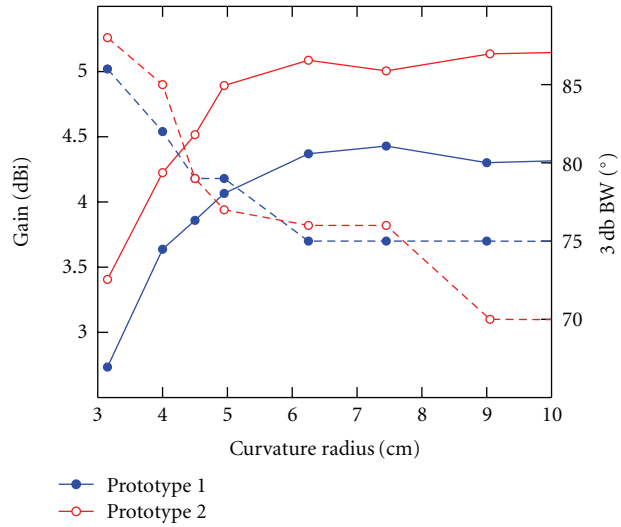

FIGURE 9: Measured gain and 3 dB beamwidth of prototypes 1 and 2 when the antennas are bent in the W_p direction. The solid lines indicate the gain along broadside, and the dashed lines show the 3 dB beamwidths.

the planar antenna) when the antenna is bent in the W_p direction. For a curvature radius of 90 mm, the measured 3 dB beamwidth is 70°, and the modeled 3 dB beamwidth is 80°. For a bending radius of 31.5 mm, the measured 3 dB beamwidth is 88°, and the modeled 3 dB beamwidth is 86°.

There is no distinct difference between the shape of the radiation patterns of prototype 1 and 2. Hence, stretching has almost no influence on the radiation pattern of bent flexible antennas. Also, from the model we conclude that the use of the corrected permittivity due to compression has almost no influence on the radiation pattern.

Figure 8 shows the modeled and measured radiation patterns in the XY plane of prototype 2 for curvature radii of 90 mm and 40 mm at a frequency of 1.573 GHz when the antenna is bent in the L_p direction. For a curvature radius of 90 mm, the measured 3 dB beamwidth is 85°, and the modeled 3 dB beamwidth is 82°. For a bending radius of 40 mm, the measured 3 dB beamwidth is 94°, and the modeled 3 dB beamwidth is 94°.

The influence of bending on the gain along broadside direction and the 3 dB beamwidth is shown in Figure 9. The measured gain and 3 dB beamwidth of prototype 1 and 2 when the antennas are bent in the W_p direction are displayed. For smaller bending radii, a decrease of the maximum gain and an increase of the 3 dB beamwidth are noticed. This effect is stronger for antennas with nonstretchable patches. The same results can be found when bending the antennas along the L_p direction.

5. Conclusion

In this paper, a novel analytical model for cylindrically bent textile patch antennas was proposed. The starting point was the existing analytical model for conformal cylindrical-rectangular patch antennas, in which additional effects due to

stretching and compression were incorporated. The model allows to calculate textile antenna performance parameters, such as resonance frequency and radiation pattern, as a function of the bending radius. Moreover, it answers the need for a fast and accurate prediction tool for bent textile patch antennas, in contrast to previously proposed measurement- or simulation-based analysis methods, which are time consuming, expensive, and do not provide physical insight into the mechanisms of bending. The resonance frequencies as a function of the bending radius can be obtained by numerically solving the cavity's dispersion relations, while the far-field patterns are given in closed-form expressions. Two main novelties were introduced in the proposed model, dedicated to the particular case of textile antennas:

(1) The patch elongation due to stretching has been derived by geometrical considerations and has been taken into account in the model.

(2) An expression for the substrate permittivity as a function of the bending radius has been proposed, which isolates the effect of bending from all other external effects.

The validity of the proposed model has been successfully verified in two ways. First, it was analytically demonstrated that for large curvature radii (i.e., for $a \to \infty$) the dispersion relations converge to the one valid for the flat state. Secondly, an experimental verification of the model was performed by means of a measurement campaign in which the resonance frequencies and the radiation patterns of five different textile patch antenna prototypes were measured for different bending radii. In particular, the new model now captures the following two effects:

(1) Concerning the resonance frequency, the measurements showed a significant variation for antennas with a nonstretchable patch and a nearly constant resonance frequency for antennas with a perfectly stretchable patch.

(2) Regarding the radiation patterns, the experiments demonstrated that stretching has almost no influence on the radiation pattern of bent flexible antennas.

In summary, an excellent agreement is now obtained between measured results and the new model.

Based on the obtained results, it can be concluded that the proposed model represents a valuable tool for textile antenna design engineers, allowing performance prediction and analysis of bent textile antennas. The model shows clear advantages with respect to previously employed methods, such as measurements and simulations, in terms of accuracy and computational cost. Moreover, it provides physical insight into bending mechanisms of textile patch antennas.

Acknowledgments

The work of F. Boeykens was supported by a doctoral grant from the Agency for Innovation by Science and Technology in Flanders (IWT). L. Vallozzi is a postdoctoral fellow of the FWO.

References

[1] P. Salonen, L. Sydanheimo, M. Keskilammi, and M. Kivikoski, "Small planar inverted-F antenna for wearable applications," in *Proceedings of the 3rd International Symposium on Wearable Computers*, pp. 95–100, San Francisco, Calif, USA, October 1999.

[2] M. Klemm, I. Locher, and G. Tröster, "A novel circularly polarized textile antenna for wearable applications," in *Proceedings of the 7th European Conference on Wireless Technology (ECWT '04)*, pp. 285–288, Amsterdam, The Netherlands, October 2004.

[3] P. J. Massey, "Mobile phone fabric antennas integrated within clothing," in *Proceedings of the 11th International Conference on Antennas and Propagation*, pp. 344–347, Manchester, UK, April 2001.

[4] A. Tronquo, H. Rogier, C. Hertleer, and L. Van Langenhove, "Robust planar textile antenna for wireless body LANs operating in 2.45 GHz ISM band," *Electronics Letters*, vol. 42, no. 3, pp. 142–143, 2006.

[5] C. Hertleer, H. Rogier, L. Vallozzi, and L. Van Langenhove, "A textile antenna for off-body communication integrated into protective clothing for firefighters," *IEEE Transactions on Antennas and Propagation*, vol. 57, no. 4, pp. 919–925, 2009.

[6] A. Bonfiglio and D. De Rossi, *Wearable Monitoring Systems*, Springer, New York, NY, USA, 2011.

[7] Y. T. Lo, D. Solomon, and W. F. Richards, "Theory and experiment on microstrip antennas," *IEEE Transactions on Antennas and Propagation*, vol. 27, no. 2, pp. 137–145, 1979.

[8] C. M. Krowne, "Cylindrical-rectangular microstrip antenna," *IEEE Transactions on Antennas and Propagation*, vol. 31, no. 1, pp. 194–198, 1983.

[9] J. S. Dahele, R. J. Mitchell, K. M. Luk, and K. F. Lee, "Effect of curvature on characteristics of rectangular patch antenna," *Electronics Letters*, vol. 23, no. 14, pp. 748–749, 1987.

[10] K. M. Luk, K. F. Lee, and J. S. Dahele, "Analysis of the cylindrical-rectangular patch antenna," *IEEE Transactions on Antennas and Propagation*, vol. 37, no. 2, pp. 143–147, 1989.

[11] J. Ashkenazy, S. Shtrikman, and D. Treves, "Electric surface current model for the analysis of microstrip antennas on cylindrical bodies," *IEEE Transactions on Antennas and Propagation*, vol. 33, no. 3, pp. 295–300, 1985.

[12] T. M. Habashy, S. M. Ali, and J. A. Kong, "Input impedance and radiation pattern of cylindrical-rectangular and wraparound microstrip antennas," *IEEE Transactions on Antennas and Propagation*, vol. 38, no. 5, pp. 722–731, 1990.

[13] D. H. Werner, R. J. Allard, R. A. Martin, and R. Mittra, "A reciprocity approach for calculating radiation patterns of arbitrarily shaped microstrip antennas mounted on circularly cylindrical platforms," *IEEE Transactions on Antennas and Propagation*, vol. 51, no. 4, pp. 730–738, 2003.

[14] T. Kellomäki, J. Heikkinen, and M. Kivikoski, "Effects of bending GPS antennas," in *Proceedings of the Asia-Pacific Microwave Conference (APMC '06)*, pp. 1597–1600, Yokohama, Japan, December 2006.

[15] L. Vallozzi, H. Rogier et al., "Radiation characteristics of a textile antenna designed for apparel application," in *Proceedings of the IEEE Galveston Bay Section Symposium for Space Applications of Wireless and RFID (SWIRF '07)*, Houston, Tex, USA, May 2007.

[16] S. Sankaralingam and B. Gupta, "Development of textile antennas for body wearable applications and investigations on their performance under bent conditions," *Progress In Electromagnetics Research B*, no. 22, pp. 53–71, 2010.

[17] I. Locher, M. Klemm, T. Kirstein, and G. Tröster, "Design and characterization of purely textile patch antennas," *IEEE Transactions on Advanced Packaging*, vol. 29, no. 4, pp. 777–788, 2006.
[18] R. F. Harrington, *Time-Harmonic Electromagnetic Fields*, McGraw–Hill, New York, NY, USA, 1961.
[19] F. W. J. Olver, D. W. Lozier, R. F. Boisvert, and C. W. Clark, "Bessel functions," in *NIST Handbook of Mathetmatical Functions*, pp. 231–232, Cambridge University Press, New York, NY, USA, 2010.
[20] *Determination of thickness of textiles and textile products*, ISO Standard 5084, 1996.
[21] C. Hertleer, A. van Laere, H. Rogier, and L. van Langenhove, "Influence of relative humidity on textile antenna performance," *Textile Research Journal*, vol. 80, no. 2, pp. 177–183, 2010.